

The Structure and Evolution of Hurricane Elena (1985). Part I: Symmetric Intensification

KRISTEN L. CORBOSIERO AND JOHN MOLINARI

Department of Earth and Atmospheric Sciences, The University at Albany, State University of New York, Albany, New York

MICHAEL L. BLACK

Hurricane Research Division, NOAA/AOML, Miami, Florida

(Manuscript received 1 December 2004, in final form 17 March 2005)

ABSTRACT

One of the most complete aircraft reconnaissance and ground-based radar datasets of a single tropical cyclone was recorded in Hurricane Elena (1985) as it made a slow, 3-day anticyclonic loop in the Gulf of Mexico. Eighty-eight radial legs and 47 vertical incidence scans were collected aboard NOAA WP-3D aircraft, and 1142 ground-based radar scans were made of Elena's eyewall and inner rainbands as the storm intensified from a disorganized category 2 to an intense category 3 hurricane. This large amount of continuously collected data made it possible to examine changes that occurred in Elena's inner-core symmetric structure as the storm intensified.

On the first day of study, Elena was under the influence of vertical wind shear from an upper-tropospheric trough to the west. The storm was disorganized, with no discernable eyewall and nearly steady values of tangential wind and relative vorticity. Early on the second day of study, a near superposition and constructive interference occurred between the trough and Elena, coincident with upward vertical velocities and the radial gradient of reflectivity becoming concentrated around the 30-km radius. Once an inner wind maximum and eyewall developed, the radius of maximum winds contracted and a sharp localized vorticity maximum emerged, with much lower values on either side. This potentially unstable vorticity profile was accompanied by a maximum in equivalent potential temperature in the eyewall, deeper and stronger inflow out to 24 km from the eyewall, and mean outflow toward the eyewall from the eye.

Within 6–12 h, intensification came to an end and Elena began to slowly weaken. Vorticity and equivalent potential temperature at 850 hPa showed indications of prior mixing between the eye and eyewall. During the weakening stage, an outflow jet developed at the eyewall radius. A strong 850-hPa updraft accompanied the outflow jet, yet convection was less active aloft than before. This feature appeared to represent a shallow, outward-sloping updraft channel associated with the spindown of the storm.

1. Introduction

The dynamics of the inner-core region of tropical cyclones (defined as the eye, eyewall, and spiral rainbands within 100 km of the center) are crucial to our understanding of hurricane intensity change. It is within this region that most of the energy generation and conversion that drives the hurricane circulation takes place (Riehl 1950; Ooyama 1969; Emanuel 1986). Despite considerable research over the last 50 yr, understanding

of the time evolution of the inner-core structure of tropical cyclones has been inhibited by the shortage of continuous observational data.

With the general lack of observations spanning a sufficiently long period of time over which the tropical cyclone evolves, observational studies of hurricane structure have commonly gone in one of two directions: 1) case studies or "snapshots" of a hurricane's structure spanning 1–3 h, or 2) construction of composites over longer periods, sometimes spanning a day or more. Landmark studies by Marks and Houze (1987), Marks et al. (1992), Franklin et al. (1993), and Reasor et al. (2000) have gone the first route by using airborne dual-Doppler data to form detailed pictures of the radial and vertical structure of hurricanes that were strengthening

Corresponding author address: Kristen L. Corbosiero, Dept. of Earth and Atmospheric Science, The University at Albany, State University of New York, 1400 Washington Ave., Albany, NY 12222.
E-mail: kristen@atmos.albany.edu

(Alicia 1983), weakening (Norbert 1984; Olivia 1994), and at peak intensity (Gloria 1985). The second method was employed by Hawkins and Imbembo (1976), Jorgensen (1984b), and Frank (1984) to construct longer-term time composites of flight-level reconnaissance data of steady Hurricane Inez (1966), weakening Hurricane Allen (1980), and rapidly intensifying Hurricane Frederic (1979). Snapshots of hurricanes show structural detail, but not time change. Composites over longer periods optimize data coverage, but might miss some important structural characteristics of intensity change.

Notable exceptions to the above are papers that have sought to document structural changes in hurricane kinematic and thermodynamic fields as intensity changes. A series of three papers by Hawkins and Rubsam (1968a,b,c) documented the life cycle of Hurricane Hilda (1964) over four consecutive days. Willoughby et al. (1982) and Willoughby (1990) examined changes in the tangential wind profiles of intensifying tropical cyclones that occurred in association with convective rings. More recently, Kossin and Eastin (2001) noted a "regime change" in equivalent potential temperature and relative vorticity in hurricanes between peak intensity and weakening.

With the increased spatial resolution in numerical models, the inner-core structure of tropical cyclones is currently being resolved with greater and greater accuracy. Using the fifth-generation Pennsylvania State University–National Center for Atmospheric Research Mesoscale Model (MM5), Braun (2002), Rogers et al. (2003), and Yau et al. (2004) have simulated realistic intensification rates and inner-core structures with model grid lengths of 1.3–2 km. However, with large variability in model outcome based on initialization of the vortex (Pu et al. 2002), boundary layer scheme (Braun and Tao 2000), and input data quality (Davis and Bosart 2002), numerical models alone are not yet sufficient to address all of the details of intensity change.

In the current study, a hurricane will be analyzed using an unusually large number of observations collected over a 55-h period during which significant changes in storm structure and intensity occurred. The goal is to provide a more complete picture of the way the inner core of a tropical cyclone evolves in time. Part I of this study focuses on the intensification process through the examination of axisymmetric fields. A future paper will concentrate on asymmetric structures with respect to environmental vertical wind shear and on observational evidence for vortex Rossby waves.

The storm chosen for this study is Hurricane Elena (1985), which made a slow anticyclonic loop in the Gulf

of Mexico while intensifying into a strong category 3 hurricane (Case 1986). Previous studies on Elena's rainfall pattern (Burpee and Black 1989), interaction with an upper-level midlatitude trough (Molinari and Vollaro 1989, 1990; Molinari et al. 1995), erratic track (Velden 1987), and tangential wind spinup (Willoughby 1990) have provided some details of Elena's evolution, but none of these previous studies has examined the evolution of Elena's inner-core structure with all available reconnaissance aircraft and ground-based radar data.

The organization of the paper is as follows. Section 2 gives details of the data used for this study. Section 3 describes the two compositing methods used to display the data. Section 4 explores the time evolution of the azimuthally averaged flight-level and ground-based radar data. Section 5 examines changes in Elena's radial and vertical symmetric storm structure that occurred during five composite time periods based on Elena's intensification rate. And finally, section 6 concludes with a summary and discussion of the results of this study, with an eye toward future work.

2. Data

a. Flight-level data

As part of a planned reconnaissance mission to study eyewall replacement cycles in tropical cyclones, the National Oceanic and Atmospheric Administration (NOAA) WP-3D N42RF and N43RF aircraft flew six separate reconnaissance missions into Elena, with a total of 88 radial passes, in the 55 h from 0100 UTC 31 August to 0800 UTC 2 September 1985. Isobaric height, temperature, dewpoint, liquid water content, wind speed and direction were recorded at 1 Hz by the instrumentation aboard the aircraft (Jorgensen 1984a). The data were transformed by personnel at the Hurricane Research Division (HRD) of NOAA into storm-relative coordinates through construction of the cyclone track by the method of Willoughby and Chelmow (1982) and interpolation of the data to a 0.5-km radial grid using a 2-km overlapping filter window. The result was a 100–150-km radial profile of the vortex structure at flight level (850 hPa in Elena) for each radial leg. In addition to the atmospheric quantities collected aboard the aircraft, radial profiles of equivalent potential temperature (Θ_e) and the symmetric vertical component of relative vorticity (ζ) were calculated, the former using the method of Bolton (1980) and the latter from the formula $\zeta = V_t/r + \partial V_t/\partial r$, with a centered differencing scheme applied to the local tangential wind (V_t).

One possible significant source of error in the flight-level thermodynamic data is instrument wetting as de-

scribed by Eastin et al. (2002a,b). Wetting of the temperature sensor by cloud droplets or rain can lead to evaporational cooling, spuriously low temperature readings, and the possibility of supersaturated thermodynamic profiles. In an attempt to reduce these errors and eliminate supersaturated temperature values, Zipser et al. (1981) proposed the following method: if the dewpoint exceeded the temperature, saturation was assumed and the dewpoint and temperature were set equal to the average of the two values. The thermodynamic data for Hurricane Elena, obtained from HRD, have been adjusted with the Zipser et al. (1981) method (hereafter referred to as the ZML correction).

Examining 666 radial legs on which concurrent measurements of temperature were available from a Barnes radiometer and Rosemount immersion thermometer, Eastin et al. (2002a) found that the ZML correction was partially effective in correcting for wetting errors, removing 30%–50% of the error. Hurricane Elena was one of the storms that Eastin et al. (2002a,b) examined for wetting errors, as the Barnes radiometer data were available on 37 of the 88 radial legs. A total of 16 wetting errors were identified on 13 of the 37 legs (M. Eastin 2003, personal communication). The mean difference between the two gauges when errors were identified was 0.66°C in temperature and 3.8 K in Θ_e , occurring most frequently in the eyewall. These values for Elena are similar to those calculated for the larger sample of storms studied by Eastin et al. (2002b), who found mean differences at 850 hPa between the datasets of 1°C in temperature and 5 K in Θ_e when wetting errors were identified.

For the Elena data, tests were performed in which the ZML-corrected temperature and dewpoint values were replaced with the Eastin et al. (2002a) values when available. As detailed in appendix A, only minor changes to the composite Θ_e profiles shown in this study were noted when the radiometer data were used. Thus, because the changes were minimal and the radiometer data were not available on all legs, all plots in this study are constructed using the HRD-supplied ZML-corrected temperature and dewpoint values.

b. Vertical incidence data

One of the WP-3D aircraft that investigated Elena carried an X-band (3.2 cm) Doppler radar that scanned a plane perpendicular to the aircraft (Jorgensen 1984a). The data collected were the radar reflectivity and the radial velocities (either toward or away from the aircraft) of the precipitation particles (Black et al. 1996). When the beam was pointing directly up or down (at its vertical incidence), the Doppler velocities collected were the vertical motions of precipitation relative to the

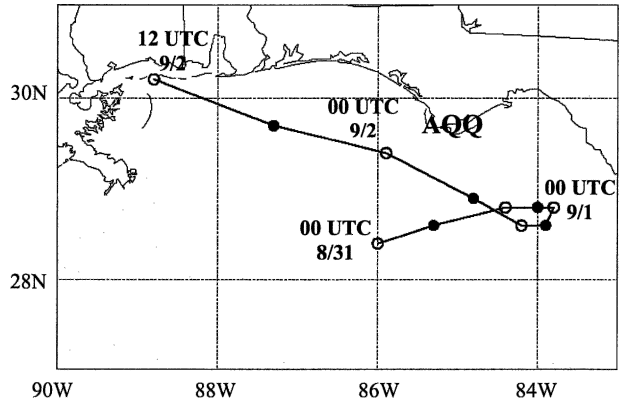


FIG. 1. TPC best track of Hurricane Elena (1985) from 0000 UTC 31 Aug to 1200 UTC 2 Sep. Open circles are the 0000 and 1200 UTC center positions and the filled circles are the 0600 and 1800 UTC positions. The location of the Apalachicola, FL, WSR-57 (AQQ) has been marked for reference.

moving aircraft. The vertical air motion was calculated by subtracting the vertical motions of the aircraft and an estimate of the precipitation particle fall speed from the raw Doppler velocities (Marks and Houze 1987). The fall speeds of the particles were computed from empirical formulas involving reflectivity, height, air density, and particle type. The uncertainty of the fall speeds can be as large as 2 m s^{-1} in updrafts in the eyewall and above the melting level due to the presence of liquid water above the 0°C isotherm (Black et al. 1994; Black et al. 1996). In convective regions, the magnitude of the true vertical motion is usually larger than the uncertainty of the fall speeds, but in stratiform regions it is not. Thus time and/or space averaging (as done in this study) must be performed to gain meaningful information about the vertical motion in these areas (Black et al. 1996).

The vertical incidence data have a horizontal resolution of 0.75 km and are averaged into 0.3-km bins in the vertical. The data may extend from the sea surface to 15 km, but Doppler data are not available within 900 m of the aircraft due to the range delay of the radar (Black et al. 1996). In Elena, flight level was 850 hPa, or ~ 1.5 km; thus the lowest level shown in the composites in section 5 will be 2.5 km.

c. WSR-57

Continuous radar scans of Elena's eyewall and inner rainbands were captured by the Weather Surveillance Radar-1957 (WSR-57) at Apalachicola, Florida (AQQ; see Fig. 1), from 2200 UTC 31 August through 0200 UTC 2 September. The radar contains a distance-dependent range correction that is constant beyond

230 km (Parrish et al. 1982). The center of Elena was within 160 km of the radar throughout the time period of study so that the inner 70 km of Elena was within 230 km of the radar at all times. The radar plots below will show reflectivity values beyond the 70-km radius, but caution must be used at these radii.

The reflectivity data were transformed from latitude–longitude coordinates to a storm-relative coordinate system with a domain of 300 km \times 300 km and a horizontal resolution of 0.75 km (Burpee and Black 1989). Radar ground clutter was removed from each scan by manually setting all data points equal to zero within a rectangle centered on the radar site that encompassed the clutter. The box was then filled by bilinearly interpolating from the adjacent rows and columns of data.

The AQQ radar made 1142 scans of Elena, with as little as 23 s between complete radar scans. This short temporal resolution was possible due to Elena's close proximity to the radar, allowing a quarter to half sweep of the radar to capture the reflectivity structure of Elena out to 150 km from the center. To have a uniform time step between radar images and to capture the mesoscale features of the reflectivity field, the scans were linearly interpolated to 5-min intervals. Only the closest two scans to the time in question were weighted and used to compute the interpolated scan. If there were no scans within 5 min of either side of the prospective interpolated time, no scan was calculated and a gap appears in the data. Short gaps in the data also appear when the radar elevation angle deviated from the nominal 0.4°. Over 95% of the scans were made at 0.4°. Alternate elevation angles (between 0.5° and 0.9°) were simply eliminated from the dataset before interpolation to the 5-min time interval.

d. Best track

Figures 1 and 2 show the Tropical Prediction Center (TPC) best-track center positions, maximum surface wind, and minimum central pressure for Hurricane Elena every 6 h from 0000 UTC 31 August to 1200 UTC 2 September. Under the influence of an approaching midlatitude trough (Case 1986), Elena moved toward the east-northeast while the intensity remained steady from 0000 to 1800 UTC 31 August. Rapid pressure falls and tangential wind spinup began just before 0000 UTC 1 September as a near superposition and constructive interference occurred between the trough and the hurricane (Molinari et al. 1995). With the trough axis situated over Elena's circulation, the steering winds above the storm weakened and the center made a slow anticyclonic loop off the western coast of Florida between 1800 UTC 31 August and 1800 UTC 1 September. Peak best-track intensity occurred between 1800 UTC 1 Sep-

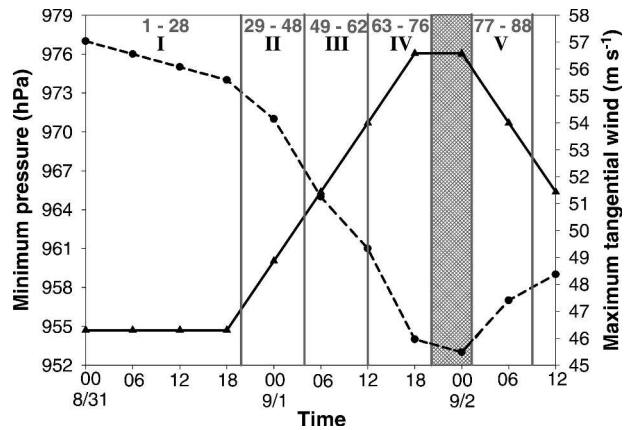


FIG. 2. TPC best-track minimum central pressure (circles and dashed line) and maximum surface wind (triangles and solid line) for Hurricane Elena (1985) every 6 h from 0000 UTC 31 Aug to 1200 UTC 2 Sep. The gray vertical lines show the breakdown of the five time periods and radial leg numbers over which the averages in section 5 were computed. The black roman numerals are the time period numbers as they are referred to in the figures and text. The gray-hatched region represents a time with no 850-hPa-level flight data.

tember and 0000 UTC 2 September as Elena began to accelerate toward the northwest and weaken through its landfall on the Alabama coastline at 1300 UTC 2 September.

e. ECMWF analyses

Environmental vertical wind shear was calculated from the European Centre for Medium-Range Weather Forecasts (ECMWF) analyses between the 850- and 200-hPa levels. Following Hanley et al. (2001), a cylindrical area-weighted average of the Cartesian components of the mean wind were computed over a radius of 500 km from the storm center. This averaging removes the symmetric vortex so that the resulting winds are a measure of cross-storm flow. Molinari et al. (1995) noted that the ECMWF analyses are particularly reliable for studying the environment of tropical cyclones within a few hundred kilometers of the extensive U.S. rawinsonde network, and Corbosiero and Molinari (2002) provide evidence that the shear from the ECMWF analyses is likely to be within 1–2 m s⁻¹ of the true vertical wind shear over 500 km of radius.

3. Methodology

In this study, the ground-based radar and 850-hPa flight-level data will be presented in two ways. The first is as radius–time Hovmöller diagrams of azimuthally averaged quantities collected from the radar and the

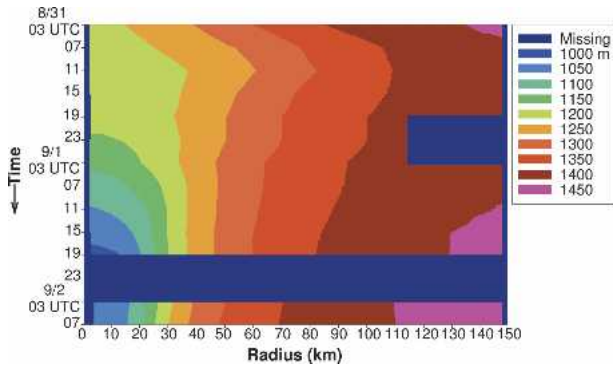


FIG. 3. Radius–time Hovmöller of azimuthally averaged 850-hPa height (m) in Elena (1985). The hours on the vertical axis represent the midpoints of the 4-h time periods over which the azimuthal averages were calculated. The dark blue shading represents radii and/or times with no flight data.

aircraft reconnaissance missions. For the ground-based radar data, the azimuthal average for each 5-min period at each radius was calculated by bilinearly interpolating the data to cylindrical coordinates, summing the reflectivity values at all azimuths for each radius, and dividing by the total number of points around (720 in this case). For azimuthal averages of the flight-level data, it was necessary to use data from multiple legs since one radial leg only provides a picture of storm structure at one azimuth. The averages were calculated by dividing the entire time period of study into 4-h bins and averaging all radial legs that occurred in each bin. The average number of legs that occurred in the fourteen 4-h windows was seven, so that each quadrant of the storm was sampled at least once. After calculation, the 4-h azimuthal averages were smoothed in radius with a nine-point Bartlett filter that removed features with wavelengths less than ~ 5 km (Jenkins and Watts 1968; Kossin and Eastin 2001). The smoothed azimuthal averages were then plotted on a radius–time Hovmöller at the midpoint of the 4-h time period over which the average was calculated; that is, the average taken between 0100 and 0500 UTC 31 August was plotted at 0300 UTC 31 August (see Fig. 3).

The decision to calculate the flight-level azimuthal averages on the basis of a constant time interval instead of after each figure-4 flight pattern was based upon the desire to capture the smooth, symmetric evolution of Elena while minimizing gaps in the data. The figure-4 was the dominant flight pattern and took between 1 and 2 h to execute in Elena. This relatively short averaging period led to irregular jumps in the azimuthally averaged tangential wind and relative vorticity. Averaging over longer periods, between 3 and 6 h, smoothed out these irregularities. The 4-h period was ultimately cho-

sen, as it was the optimum choice between time resolution and sufficient data to define an azimuthal average.

The reconnaissance aircraft data will also be presented as averages over five significant time periods in Elena's evolution. The choice of the number and divisions between time periods was determined by natural breaks between reconnaissance missions and by examining the evolution of the best-track surface wind trace (Fig. 2). The gray vertical lines in Fig. 2 show the breakdown of the five time periods and radial leg numbers over which the averages were computed. Time period I, legs 1–28, captured Elena as a nearly steady category 2 storm. Storm structure at the beginning of deepening was illustrated by time period II, legs 29–48. The middle of deepening was captured by time period III, legs 49–62. Time period IV, legs 63–76, showed Elena at or near the time of peak intensity. Finally, time period V, legs 77–88, showed the storm to be weakening after a 5-h break during which there were no flights into Elena. Radial legs 87 and 88 will be used only in the composites of vertical incidence data and not in flight-level composites as the reconnaissance aircraft deviated from the 850-hPa level during these last two legs.

The five composite periods defined above are computed over time spans of 8 to 20 h, over which significant variations can occur in the radius of maximum winds (RMW). To avoid the potential smearing of details that may come from the calculation of a straight radius composite, the flight data will be composited on a single, meaningful radius named the radius of maximum slope change (RMSC). In each leg this radius was determined to be the distance from the center where the 850-hPa tangential wind stopped increasing rapidly with increasing radius. This radius was typically close to both the inner edge of the eyewall and the radius of maximum updraft. Appendix B contains details about the choice and significance of the RMSC. In each time period the radial legs were aligned according to distance from the RMSC, and then a simple average was computed at each radius. Before plotting, the time period or quadrant averages were smoothed in radius with the nine-point Bartlett filter.

4. Radius–time Hovmöllers

The radius–time Hovmöller of the azimuthally averaged height of the 850-hPa surface is shown in Fig. 3. Between the time periods centered on 0300 and 1100 UTC 31 August, the height of the 850-hPa surface fell by approximately 30 m everywhere inside the 150-km radius. During the next 12 h, heights outside the 40-km radius began to increase, while values in the core began

to fall slowly. Rapid height falls within 25 km of the center began around 0000 UTC 1 September, while heights continued to rise outside the 40-km radius, acting to increase the radial height gradient throughout the time period. The magnitude of these height rises is on par with those found by Willoughby et al. (1982) during the intensification of Hurricanes Anita (1977), David (1979), and Allen (1980). The plot shows that the minimum 850-hPa height was recorded during the time period centered on 1900 UTC 1 September.

Figure 4 shows the radius–time Hovmöller of the 850-hPa tangential wind speed, overlaid with the time evolution of the RMW. The maximum tangential wind at 850 hPa decreased and the RMW moved outward to the 80-km radius between 0300 and 1100 UTC 31 August, consistent with the decreasing radial height gradient at 850 hPa seen in Fig. 3. Over the next 12 h, Elena strengthened slowly as the RMW contracted and then fluctuated around the 70-km radius. Between the time periods centered on 0300 and 0700 UTC 1 September, a 25-km decrease, or jump, in the RMW occurred because the rapid spinup at inner radii that began ~0000 UTC 1 September exceeded the spinup that was occurring at outer radii. The peak azimuthal mean tangential winds at 850 hPa were recorded much later, between 0300 and 0700 UTC 2 September, after the best-track peak intensity (Fig. 2). However, it is worth noting that the maximum 850-hPa wind speed may have actually occurred between 2100 UTC 1 September and 0200 UTC 2 September (see Fig. 2) when no flight-level data were available. Evidence for this will be presented in the next section.

The time evolution of the symmetric relative vorticity and the radius of maximum vorticity are shown in Fig. 5. The radial distribution of relative vorticity was quite broad and exhibited little change in structure until Elena started to intensify around 0000 UTC 1 September,

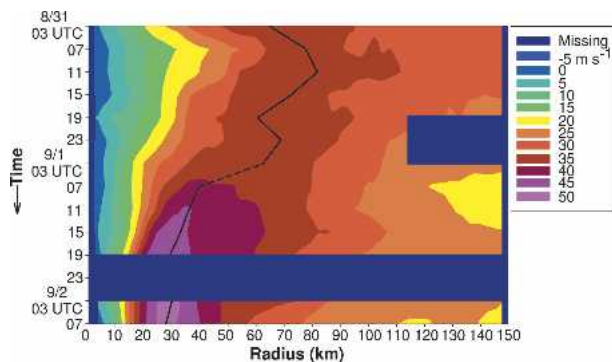


FIG. 4. Same as Fig. 3, except for tangential wind (m s^{-1}) at 850 hPa. The solid black lines show the time evolution of RMW. The dashed line depicts a jump or redevelopment of the RMW.

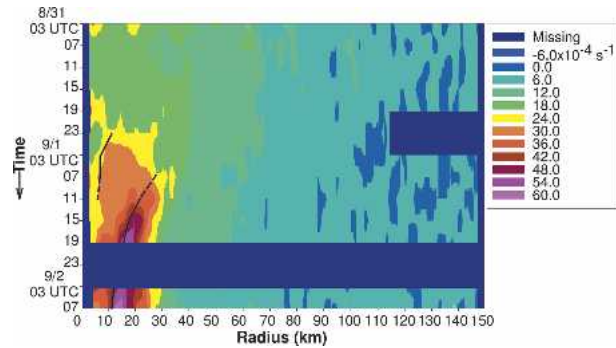


FIG. 5. Same as Fig. 3, except for relative vorticity ($\times 10^{-4} \text{ s}^{-1}$). The solid black lines show the time evolution of the radius of maximum vorticity, while the dashed lines track the evolution of the two distinct vorticity maxima.

when values started to increase approximately 15 km from the eye. This inner maximum increased in magnitude and moved slowly inward to the 10-km radius between 2300 UTC 31 August and 0700 UTC 1 September, after which it remained nearly stationary and weakened during the next 4 h. Around 0700 UTC 1 September, a second vorticity maximum developed at the 30-km radius. This maximum formed in response to the tangential wind profile (Fig. 4) becoming much more peaked due to a large increase in the wind on the inner edge of the eyewall. This new vorticity maximum became the sole maximum after 1100 UTC 1 September, when values of vorticity increased rapidly in a 5–7-km-wide ring on the inner edge of the eyewall that moved radially inward with time to the 15-km radius and attained vorticity values greater than $60 \times 10^{-4} \text{ s}^{-1}$.

The radius–time Hovmöller of azimuthally averaged ground-based radar data from Apalachicola, Florida, is shown in Fig. 6, overlaid with the RMW and radius of maximum vorticity from Figs. 4 and 5, respectively. Recall that the radar data do not begin until 2200 UTC 31 August, just before Elena started to rapidly intensify. Between 2200 UTC 31 August and 0200 UTC 1 September, reflectivities >20 dBZ were sometimes seen within the developing eye of Elena, near the radius of maximum vorticity. Maximum values of reflectivity were seen around the 80-km radius, collocated with the RMW. After 0200 UTC 1 September, the eye cleared of precipitation and the radius of maximum reflectivity and the RMW could be traced moving inward with time. As deep convection became concentrated in the eyewall between 0300 and 0700 UTC 1 September, rapid spinup occurred and the radius of maximum vorticity became anchored to the inner edge of the eyewall, after which the RMW and radius of maximum vorticity remained within 15 km of each other. After 1200 UTC 1 September, the maxima in all three fields contracted

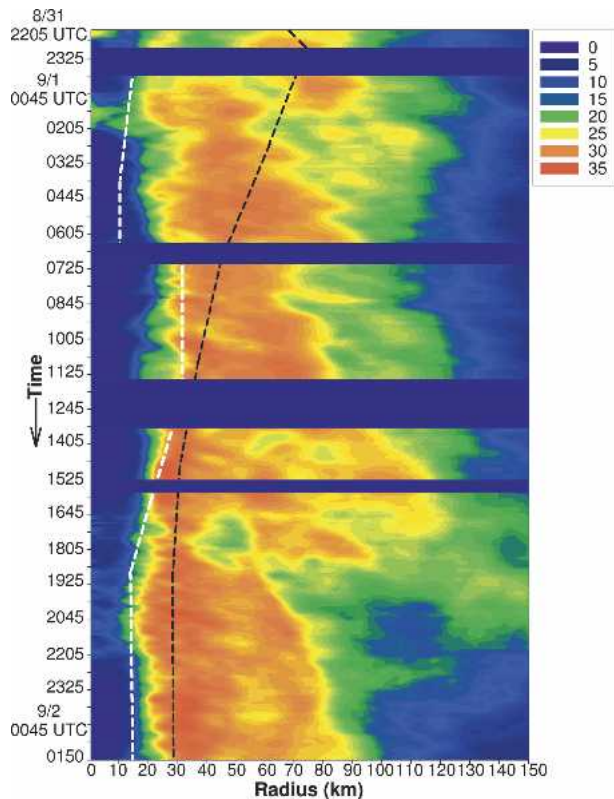


FIG. 6. Radius-time Hovmöller of azimuthally averaged reflectivity from the WSR-57 Apalachicola, FL, radar from 2205 UTC 31 Aug to 0150 UTC 2 Sep. Times with no data are indicated by the dark blue strips. The dashed black line is the radius of maximum wind from Fig. 4 and the dashed white line is the radius of maximum vorticity from Fig. 5.

with time, with the RMW and radius of maximum reflectivity reaching their smallest values around 2100 UTC 1 September, at or near the time of best-track peak intensity. The radius of maximum reflectivity and the RMW began to slowly retreat after 2100 UTC 1 September, during the period in which the 850-hPa heights began to rise inside the 20-km radius (Fig. 3). Interestingly, the radius of maximum vorticity continued to decrease during this time period, slowly moving into the eye.

After approximately 0700 UTC 1 September, the evolution of Elena is broadly consistent with the results of Shapiro and Willoughby (1982), confirmed by Willoughby et al. (1982) and Willoughby (1990), who used Eliassen's (1951) diagnostic framework to evaluate the balanced vortex response to imposed point sources of heat or momentum. With a heat (or momentum) source placed at the RMW, Shapiro and Willoughby (1982) found rapid height falls everywhere inside the source radius, with the largest height falls in the center of the vortex, and little to no change in heights at radii greater

than 1.3 RMW. The greatest spinup of tangential winds was noted to occur just radially inside the RMW, acting to contract the wind maximum as the storm intensified. To illustrate how the source of heating in Elena may have evolved, Fig. 7 shows the azimuthally averaged AQQ radar data from Fig. 6 time averaged into 4-h bins to match the averages of the flight data shown in Figs. 3–5. Although the averages were calculated for each 4-h period for which the radar data were available, Fig. 7 only shows the average reflectivity for the time periods centered on 2300 UTC 31 August and 0700 and 1500 UTC 1 September to highlight the evolution of the reflectivity field. In the time period centered on 2300 UTC 31 August, Fig. 7 shows that there were two reflectivity maxima, the first, and smaller of the two, at the 25-km radius, and the second, larger maximum at 75 km. It is hypothesized that this outer reflectivity maximum, used as a proxy for heating, was responsible for maintaining the flat wind profile and RMW out near the 75 km on 31 August. Starting in the time period centered on 0300 UTC 1 September (not shown) and continuing through the time centered on 0700 UTC 1 September, a significant change occurred to the radial profile of reflectivity where only one maximum was noted, initially at the 45-km radius and moving inward with time to the 25-km radius by 1500 UTC. The shift from two maxima of heating to a single maximum in the eyewall was coincident with the beginning of height falls within the eye of Elena (Fig. 3), and the rapid spinup of the tangential wind (Fig. 4). After this shift to a concentrated area of heating, intensification progressed similar to the diagnostic framework of Shapiro and Willoughby (1982).

The evolution of Elena discussed above is also consistent with the trough interaction and superposition hypothesis of Molinari and Vollaro (1989, 1990) and

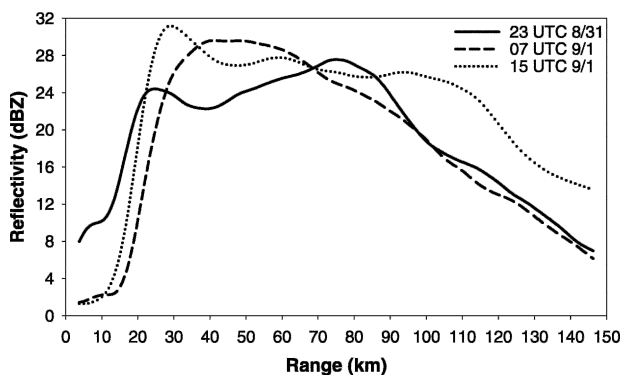


FIG. 7. Azimuthally averaged ground-based radar data from Fig. 6, time averaged in 4-h bins to match the flight-level radius-time Hovmöllers shown in Figs. 3–5. The curves are labeled as the midpoint of each 4-h average.

TABLE 1. Middle column: environmental vertical wind shear between 850 and 200 hPa, averaged within 500 km of the center of Hurricane Elena, calculated using gridded analyses from the European Centre for Medium-Range Weather Forecasts. Right column: minimum central pressure and maximum surface wind from Tropical Prediction Center's best-track dataset.

Time	Vertical wind shear	Minimum pressure/maximum wind
0000 UTC 31 Aug	300° at 9.7 m s ⁻¹	977 hPa/46.3 m s ⁻¹
1200 UTC 31 Aug	280° at 9.4 m s ⁻¹	975 hPa/46.3 m s ⁻¹
0000 UTC 1 Sep	324° at 4.2 m s ⁻¹	971 hPa/48.9 m s ⁻¹
1200 UTC 1 Sep	316° at 8.5 m s ⁻¹	961 hPa/54.0 m s ⁻¹
0000 UTC 2 Sep	326° at 6.5 m s ⁻¹	953 hPa/56.6 m s ⁻¹
1200 UTC 2 Sep	346° at 6.4 m s ⁻¹	959 hPa/51.4 m s ⁻¹

Molinari et al. (1995). On 31 August, Elena initially weakened (Figs. 3 and 4) under the influence of strong environmental vertical wind shear ($>9 \text{ m s}^{-1}$; Table 1) from the approaching upper-level trough. Nearly steady conditions or slight strengthening occurred late on 31 August as the upper trough approached the hurricane and the shear began to weaken. Rapid height falls (Fig. 3) began around 0000 UTC as the vertical wind shear dropped to 4 m s^{-1} over the center (Table 1), and a near superposition and constructive interference occurred between the trough and Elena. After 0000 UTC 1 September, a significant increase in reflectivity was noted (Figs. 6 and 7), lending evidence to the hypothesis of Molinari et al. (1995) that diabatic heating from Elena eroded the potential vorticity (PV) anomaly associated with the trough and prevented it from crossing the storm center, thus allowing the low-shear environment to persist and Elena to rapidly intensify for the next 18 h (Figs. 3–5).

5. Changes in radial and vertical structure with intensification

In this section, composites of various reconnaissance flight variables over the five significant time periods described in section 3 will be shown. The composites below are not straight radius composites, but rather are shown with respect to the RMSC discussed in section 3 and expressed as distances away from that radius. Negative values will be used to indicate radii inside the RMSC, and positive values radii outside the RMSC. Only the area -18 to $+60$ km from the RMSC will be shown as these distances approximately represent the radii where data coverage was greater than 75% (i.e., greater than 75% of the legs that made up each composite sampled that radius).

a. 850-hPa flight-level data

Figure 8a shows the average 850-hPa tangential wind profiles for each of the five composite time periods. Winds decreased slightly at all radii out to 30 km from the RMSC between time periods I and II. As Elena intensified during time periods II through IV, winds decreased in the eye (-6 to -18 km from the RMSC), while winds increased -6 to $+42$ km from the RMSC, with the greatest spinup located just outside the RMSC. Between periods IV and V, the winds increased within the eye of Elena, a sign that intensification may have ended as shown by Kossin and Eastin (2001). Nevertheless, the winds continued to spin up at the RMSC, and spindown at radii greater than $+18$ km from the RMSC, creating a more peaked wind profile. Thus, even as the best-track data showed Elena to be weaker at the surface on 2 September (Fig. 2), the 850-hPa tangential wind continued to increase.

Figure 8b shows the average relative vorticity in each of the five time periods. Values increased steadily with time inward of $+6$ km from the RMSC during time periods I–III, with the core of Elena in a near state of solid-body rotation, but with a small peak in vorticity 2–3 km inside the RMSC. The transition between periods III and IV was dramatic, with a suppression of high-vorticity values in the core, and a sharp rise just inside the RMSC to $60 \times 10^{-4} \text{ s}^{-1}$. Between time periods IV and V, after peak intensity, vorticity values decreased near the RMSC and rose to their highest levels 8 km inward of the RMSC. Time period IV was the only one with a ring of high vorticity surrounded by much lower values on either side. Recent numerical modeling work by Schubert et al. (1999) has shown that such annular vorticity profiles can support barotropic instability and the growth of unstable modes that can lead to asymmetric horizontal mixing between the eye and eyewall. This mixing increases vorticity in the eye and decreases values in the eyewall, as seen during time period V.

Figure 8c shows the average 850-hPa radial wind in each of the five composite time periods. At this level Elena exhibited outflow at all times and radii, except for time period IV when inflow extended out to $+25$ km from the RMSC and converged with outflow from the eye near the RMSC. A sharp reversal in radial wind occurred between time periods IV and V with outflow replacing inflow 0 to $+24$ km from the RMSC, with a peak in outflow, or an outflow jet, at the RMSC.

The depth and strength of the low-level inflow in tropical cyclones has been found to vary significantly from storm to storm and within the same storm depending on storm intensity. Hawkins and Rubsam (1968b),

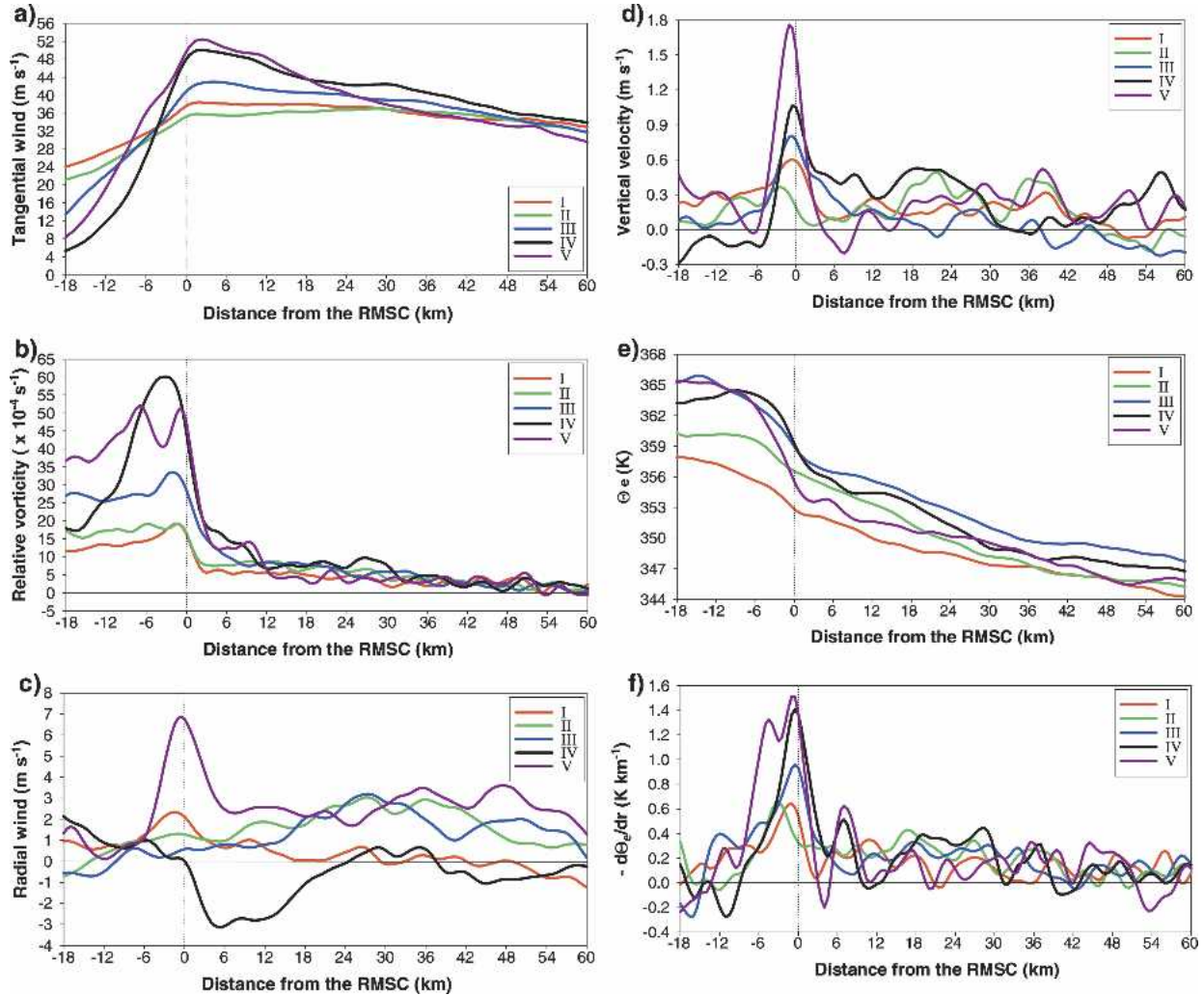


FIG. 8. Average (a) tangential wind (m s^{-1}), (b) relative vorticity ($\times 10^{-4} \text{ s}^{-1}$), (c) radial wind (m s^{-1}), (d) vertical velocity (m s^{-1}), (e) equivalent potential temperature (K), and (f) radial gradient of equivalent potential temperature (K km^{-1}), in each of the five time periods shown in Fig. 2, composited with respect to the RMSC.

Hawkins and Imbembo (1976), and Marks and Houze (1987) all documented strong inflow from the surface to at least the 750-hPa level in hurricanes that were deepening or at peak intensity. At 850 hPa, outflow from the eye to the eyewall and weak inflow outside the eyewall have been noted by Frank (1984), Jorgensen (1984a,b), Willoughby et al. (1984), and Franklin et al. (1993) in Hurricanes Frederic (1979), David (1980), Gert (1981), and Gloria (1985) during intensification and at the time of peak intensity, similar to time period IV in Elena. A dramatic reversal of the flow pattern occurred during time period V in Elena with a peak in outflow noted at the RMSC, similar to both the weakening stages of Hurricanes Norbert (1984) and Olivia (1994) documented by Marks et al. (1992) and Reasor et al. (2000), respectively, and the balanced spindown simulations of Montgomery et al. (2001).

Figure 8d shows the average flight-level vertical motion in each of the five composite time periods with respect to the compositing radius. In all time periods except for the beginning of intensification (time period II), the maximum composite updraft in Elena was within 2 km of the RMSC, again giving dynamical significance to the RMSC as choice of compositing radius. The composite updraft grew in magnitude with time as Elena intensified, and continued to increase after peak intensity to a value of 1.8 m s^{-1} during time period V. Significant subsidence occurred within the eye only during time period IV. The magnitude of the subsidence in the composite exceeded -0.1 m s^{-1} only one other time: from +6 to +10 km from the RMSC during the last time period.

A strong, organized updraft channel on the inner edge of the eyewall with flanking downdrafts on one or

both sides has been noted in several observational and modeling studies of tropical cyclones (e.g., Shea and Gray 1973; Jorgensen et al. 1985; Yau et al. 2004; Wu et al. 2005). The peak composite upward vertical velocity of 1.8 m s^{-1} in Elena is smaller than the time-averaged vertical velocities of $2\text{--}4.5 \text{ m s}^{-1}$ noted by Jorgensen (1984a,b), but on par with Black et al.'s (1996) study in which more than 70% of the vertical velocities recorded in the eyewall were between 2 and -2 m s^{-1} , and with Eastin et al.'s (2005) finding that the average convective updraft in the eyewall was 2.2 m s^{-1} at 850 hPa. Peak downdrafts in excess of -10 m s^{-1} were recorded at 850 hPa in Elena, but the composite downdraft magnitude does not exceed -0.3 m s^{-1} due to the lack of a preferred radius for downdrafts with respect to the RMSC and weaker magnitudes of downdrafts overall. Similar results have been noted by Jorgensen (1984b), Jorgensen et al. (1985), and Black et al. (1996).

Figure 8e shows the average equivalent potential temperature (Θ_e) during the five composite time periods with respect to the RMSC. During the first three time periods, values of Θ_e increased at all radii, with peak values well inside the RMSC, at or near the storm center. During time period IV, the largest values of Θ_e developed outside the storm center, just inside the RMSC. The peak returned to the eye during time period V. As Elena weakened at 850 hPa during time period V, values of Θ_e decreased by $\sim 5 \text{ K}$ over the 30 km of radius between -6 and $+24 \text{ km}$ from the RMSC. This significant drop in Θ_e over a wide radial range could reflect the intrusion of dry air from land or the storm moving over cooler SSTs due to its proximity to the coast. Alternately, the drop could be due to the occurrence of instrument wetting errors (Eastin et al. 2002a) during time period V due to the enhanced low-level eyewall updraft and reflectivity (Figs. 8d and 9c).

Values of Θ_e decreased during time periods IV and V outside the RMSC, sharply increasing the radial gradient of Θ_e . This increase in the radial gradient of Θ_e is quantified in Fig. 8f. The largest radial gradient of Θ_e was found within 3 km of the RMSC during all time periods, attaining maximum value during time period V. The maximum radial gradient of Θ_e at 850 hPa is thus nearly coincident with the maximum composite updraft in both magnitude and location. Hawkins and Imbembo (1976) and Frank (1984) found the radial gradient of Θ_e is maximized within the eyewall, and the increase in the gradient with intensification lends evidence to Emanuel's (1997) argument of the eyewall as a front.

Many observational and numerical modeling studies that have examined the radial distribution of Θ_e in hur-

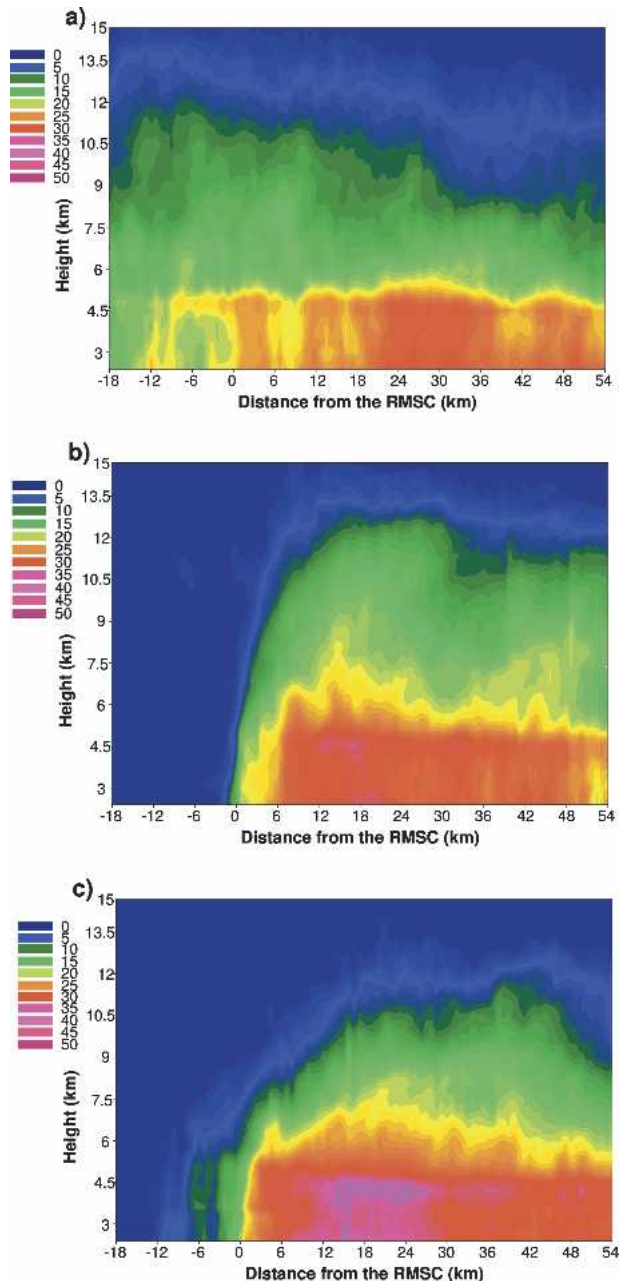


FIG. 9. Radius–height composites of vertical incidence Doppler-derived radar reflectivity (dBZ) with respect to the 850-hPa RMSC for time periods (a) II, (b) IV, and (c) V, shown in Fig. 2.

ricanes have found maximum values within the eye (Hawkins and Imbembo 1976; Frank 1984; Liu et al. 1999), just as in four of the five composite time periods in Elena. Other studies have found the highest values of Θ_e in the eyewall (Kossin and Eastin 2001; Braun 2002). Kossin and Eastin (2001) found maximum values of Θ_e in the eyewall during intensification, but a transition to the highest values in the eye after intensification had

stopped, which they attributed to mixing between the eye and eyewall. Values of Θ_e were also noted to increase in the eye after intensification had ended by Willoughby (1998) as the height of the inversion separating warm, dry air above, from cooler, moist air below, rose from below to above the aircraft observational level. As data from only one flight level was collected in Elena, the relative roles of mixing and changes to the inversion height in the evolution of Θ_e remains uncertain.

b. Vertical incidence data

In Elena, only three composite radar reflectivity radius–height plots were constructed as compared to the five composite time periods discussed above for the flight-level data. This is due to the fact that the tail radar, which captures the Doppler velocities and reflectivities, was only installed on one of the two NOAA P-3 aircraft in 1985. The time periods for the three composites are shown in Fig. 2 and encompass legs 29–48 (time period II), 63–76 (IV), and 77–88 (V), respectively. The data are again composited with respect to the RMSC at 850 hPa, and only the radii and heights where 75% of the legs contain data are plotted. While both radar reflectivity and vertical velocity data are available from the vertically pointing Doppler, only the composite reflectivity plots will be shown below. Time period averages of the vertical velocity data were made, but differences in updraft slope and position between the upshear and downshear halves of Elena were too large to illustrate any true “composite” vertical velocity structure.

Figures 9a–c show the composite radar reflectivity radius–height diagrams for time periods II, IV, and V, respectively. The first composite shows Elena to be a disorganized category 2 hurricane with clouds and precipitation located well inward of the RMSC and no well-defined eye or eyewall. Consistent with previous studies of tropical cyclone precipitation structure (e.g., Jorgensen 1984a; Black et al. 1996), the bright band was seen by the enhanced swath of reflectivity at a height of 4.5 km and the sharp gradient in reflectivity above. The highest values of reflectivity at this time were found 24–36 km outside the RMSC.

Figure 9b shows that the reflectivity pattern had undergone a dramatic change between time periods II and IV. A precipitation-free eye had developed and a well-defined eyewall existed with its inner edge at the 850-hPa RMSC. The highest values of reflectivity were found within and below the bright band at the 5-km height, 18 km outside the RMSC. As a measure of storm intensity and convective vigor, the slope of the eyewall from the vertical, measured by the slant of the 10-dBZ contour (Jorgensen 1984a), was noted to be 30°

in the 0–6-km level and 46° from 6 to 12 km (the slopes appear to be smaller in the figure due to a lack of a 1:1 height to radius ratio).

Finally, during time period V (Fig. 9c), significant changes occurred to the reflectivity within the eyewall region. Evidence of reflectivity >10 dBZ in the eye might indicate mixing between the eye and eyewall. The inner edge of the eyewall was still well defined at the RMSC but the height of the eyewall clouds had been substantially reduced. Outside the eyewall, values of reflectivity had increased to their highest values, with maximum values of over 40 dBZ located in the bright band between 12 and 24 km from the RMSC. The slope of the eyewall had increased at mid- and upper levels, as the 6–12-km slope was now 74° from the vertical, while the 0–6-km slope remained nearly unchanged at 34°.

Since tropical cyclones are warm-core vortices in approximate hydrostatic and gradient wind balance, surfaces of angular momentum must slope radially outward with height (Emanuel 1986). Following Houze (1993), the outward slope of a momentum surface can be expressed as $\partial r/\partial p|_m = (\partial m/\partial p)/(\partial m/\partial r)$, where r is radius, p is pressure, and m is momentum. Substituting in the thermal wind equation, ideal gas law, and the definition of absolute vorticity in cylindrical coordinates, the outward slope of a momentum surface is directly proportional to the radial gradient of temperature and inversely proportional to absolute vorticity. Many authors have noted the lower portion of the eyewall to be nearly vertical (due to large vorticity), sloping appreciably outward only above 6–8 km (due to decreasing vorticity and larger radial gradients of temperature in the midtroposphere) (Hawkins and Imbembo 1976; Marks 1985; Black et al. 1994), similar to Elena in Figs. 9b and 9c. The large increase in slope between Figs. 9b and 9c could also be explained in this manner, as spin-down of the vortex during time period V, which is initially largest at midlevels (i.e., Reasor et al. 2000), would result in lower values of vorticity and an increase in slope. Alternately, the significant decrease in Θ_e from the RMSC out to 24 km from the RMSC during time period V indicates that air coming into the eyewall updraft could have lower values of Θ_e , be less buoyant, and thus turn outward at a much lower height (Fig. 8c).

6. Summary and discussion

Aircraft reconnaissance and ground-based radar data were used to examine the evolution of the symmetric radial and vertical structure of Hurricane Elena (1985). Under the influence of an approaching midlatitude trough, Elena was a disorganized, category 2 hurricane

that had no discernable eyewall (Fig. 9a), nearly steady values of vorticity (Fig. 5) and tangential wind (Fig. 4), and broad, weak outflow (Fig. 8c) at 850 hPa on 31 August. As detailed by Molinari et al. (1995), a near superposition and constructive interference occurred between Elena and the trough early on 1 September, initiating pressure falls within 25 km of the center (Fig. 3) and spinup of the tangential wind 30–40 km outside the eye (Fig. 4). Between 0300 and 0700 UTC 1 September, upward vertical velocities and the radial gradient of reflectivity became concentrated around the 30-km radius, leading to the formation of an eyewall (Fig. 7). Continued spinup of the tangential wind caused an inward jump of the RMW (Fig. 4) and the development of a vorticity maximum on the inner edge of the eyewall (Fig. 6).

Late on the 1 September, around the time of peak intensity, a sharp vorticity maximum was evident just inside the RMSC (Fig. 8b), with much lower values on either side, indicating a likely unstable vorticity profile (Schubert et al. 1999). Substantial inflow occurred within 24 km of the RMSC with outflow from the eye to the eyewall (Fig. 8c). The maximum values of Θ_e were well inside the core at the time and the radial gradient of Θ_e had increased significantly (Fig. 8f). This pattern of radial flow and evolution of Θ_e are suggestive of Emanuel's (1997) frontal collapse of the eyewall.

Early on the 2 September, after a 5-h gap with no flight-level data, the sharply peaked vorticity profile had vanished (Fig. 8b), largely due to increased values within the eye. The largest values of Θ_e were also found within the eye at this time (Fig. 8e), although the change was more subtle than the transition in vorticity. The transitions in these fields are suggestive of asymmetric mixing between the eye and eyewall due to the barotropic instability of the annular vorticity profile seen during time period IV (Schubert et al. 1999). The transitions in Elena were however, much weaker than those documented by Kossin and Eastin (2001), who showed Θ_e increases of 10–15 K in the eye, and a complete relaxation of the vorticity profile to a monopole.

Paradoxically, although the storm was weakening in terms of surface winds (Fig. 2), the 850-hPa tangential wind (Fig. 8a) and vertical velocity maxima (Fig. 8d) were stronger during time period V. Contrary to this stronger low-level eyewall updraft, however, the vertical incidence profile during time period V (Fig. 9c) showed that the depth of the eyewall convection was greatly reduced. Additionally, the radial wind exhibited a peak in outflow at the RMSC during time period V (Fig. 8c). A framework for understanding these changes in storm structure comes from the numerical simulations of Montgomery et al. (2001) who tested Eliassen

and Lystad's (1977) balanced spindown theory. Montgomery et al. (2001) showed that an outflow jet, unpredicted by theory, was evident just above the boundary layer in weakening symmetric vortices. The outflow was driven by enhanced convergence in the boundary layer and a strong eyewall updraft that diverged aloft, ultimately leading to faster spindown of the vortex. Very similar conditions were noted during time period V in Elena, with peak upward vertical motion in the eyewall and a divergence (not shown) of $1.8 \times 10^{-3} \text{ s}^{-1}$ located 3 km inside the RMSC, a value 6 times larger than at any radius in any previous time period. Thus the peak in outflow and enhanced upward motion at the RMSC seen during time period V are hypothesized to be a reflection of a shallow, outward sloping updraft channel forced by enhanced boundary layer convergence. Lower values of Θ_e in the eyewall during time period V also support this idea, as the reduced buoyancy makes it much more likely that the rising air will turn outward.

The life cycle of intensity change in Elena appears to proceed as follows: during intensification, Θ_e and its radial gradient near the eyewall steadily increased. The RMW and radius of maximum vorticity contracted in a manner consistent with Shapiro and Willoughby (1982), and an annular vorticity maximum developed and strengthened in the eyewall. Thereafter, evidence suggests that eyewall became barotropically unstable and mixed high values of vorticity and Θ_e from the eyewall into the eye. This mixing appeared to act as a break on intensification, as suggested by Schubert et al. (1999) and Kossin and Eastin (2001). Subsequently, vortex spindown was accompanied by an 850-hPa outflow jet, indicative of a strongly tilted shallow circulation like that described by Montgomery et al. (2001), which further enhanced spindown of the vortex.

While this paper focuses on the evolution of Elena's symmetric storm structure through the use of azimuthal and time averages, Elena did possess significant asymmetries in radial and vertical structure as alluded to earlier. Fortunately, the unusually large amount of radar and reconnaissance data collected in Elena make it possible to examine the convective, kinematic, and thermodynamic asymmetries that existed within the storm core. In Part II of this paper, the asymmetries in Elena will be linked to direction and strength of the vertical wind shear of the environment and to vortex Rossby wave activity during the time of mixing between the eye and eyewall.

Acknowledgments. The authors thank the flight crews and research scientists from NOAA's Aircraft Operations Center and Hurricane Research Division

for their dedicated efforts to collect the reconnaissance data used for this study. We are indebted to David Vollaro for his help in developing computer programs to read and plot the best-track data, and to Matthew Eastin for providing the Elena radiometer temperature data. We also would like to thank Jim Kossin and an anonymous reviewer for helpful comments that improved the quality of the manuscript. This work was supported by NSF Grants ATM-0418682 and ATM-0000673.

APPENDIX A

Instrument Wetting Errors

The side-looking radiometer data that Eastin et al. (2002a,b) used to identify wetting errors in 31 Atlantic and east Pacific hurricanes were available on 37 of the 88 radial legs in Elena. The data were available on legs 15–18, 20, 22–26, and 50–76, covering part or all of composite time periods I, III, and IV (Fig. 2). As the focus of this study was to examine either time or azimuthal averages of the flight-level data, the averaging of several values of temperature (or Θ_e) at one radius will, presumably, act to mitigate the effects of wetting errors to the mean profile. As a test, mean Θ_e profiles were computed by substituting the corrected (radiometer) temperature values of Eastin et al. (2002a,b) for the ZML-corrected data when available. The maximum difference in the composite Θ_e values over the three time periods defined in Fig. 2 with the use of the radiometer data was 2.3 K, located 3–6 km outward of the mean eyewall updraft position. As shown in section 5, these differences are smaller than the changes in thermal structure that occurred as a result of Elena's intensification.

Figure A1 shows the average Θ_e calculated using only the ZML-corrected data and using the radiometer

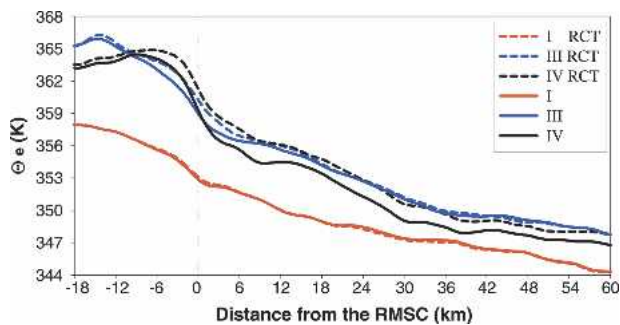


FIG. A1. Average equivalent potential temperature (K) for time periods I, III, and IV calculated from the radiometer (RCT) data of Eastin et al. (2002a,b) (dashed curves) and from the ZML-corrected data (solid curves).

data when available for time periods I, III, and IV. There is almost no change to the average Θ_e in time period I, due to the fact that less than half of the 28 legs that made up the average had radiometer data. The maximum difference between the radiometer and Rosemount values was noted in time period III between +3 and +12 km from the RMSC, and the peak value shifted slightly inward from -6 to -9 km from the RMSC, but remained in the eyewall with a pronounced decrease in toward the eye. During time period IV the largest errors were found between -6 and +3 km from the RMSC, while the maximum value of Θ_e remained at -15 km from the RMSC.

Thus, since the radiometer temperature data were not available on all legs, the changes to the composite Θ_e and radial gradient of Θ_e profiles were relatively small, and the conclusions the same when the radiometer data were used, all composites in this study were calculated from the ZML-corrected temperature and dewpoint values.

APPENDIX B

Choice and Significance of Compositing Radius

To composite the flight-level and vertical incidence data on a single meaningful radius, the tangential wind trace from each radial leg was examined and the radius where the tangential wind stopped increasing rapidly with increasing radius was determined. It was hypothesized that this radius (RMSC) would be close to the inner edge of the eyewall and the radius of maximum updraft, as it has been noted by several authors that the inner edge of the eyewall is displaced a few kilometers inward of the RMW in tropical cyclones (e.g., Shea and Gray 1973).

Figure B1 shows two examples of how the RMSC was chosen and its position relative to the RMW. During radial leg 29 (Fig. B1a; 2003–2015 UTC 31 August), Elena exhibited a nearly monotonic increase in tangential winds from the center to the ~50 km radius, after which the tangential wind increased more rapidly to the 55-km radius. The wind profile then increased much more slowly to the RMW at 78 km. In this case, the RMSC was assigned to the 55-km radius. It is notable that the RMSC and the RMW differed by more than 25 km at this time. Similar shaped profiles were common in Elena until the storm started to rapidly intensify after 0300 UTC 1 September (radial leg 48), when the RMW jumped inward by some 25 km (see Fig. 4).

Figure B1b shows the radial wind profile during leg 65 (1403–1425 UTC 1 September) that is much more typical of a rapidly deepening hurricane. The winds increased sharply from the core to the ~20 km radius and

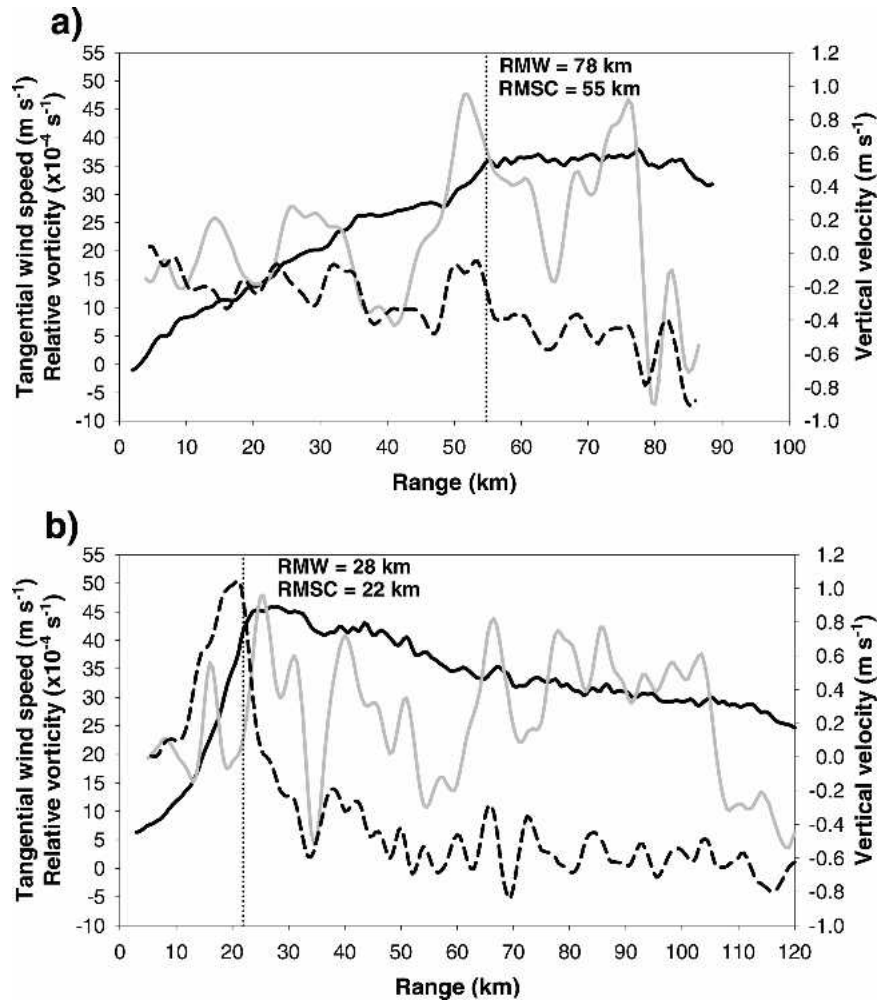


FIG. B1. The 850-hPa tangential wind, smoothed relative vorticity, and smoothed vertical velocity profiles from (a) leg 29 and (b) leg 65 into Hurricane Elena (1985) detailing how the compositing radius was chosen.

decreased slowly beyond. The RMSC is thus located at 22 km and the RMW is at 28 km.

Also shown in Fig. B1 are the radial profiles of relative vorticity and vertical motion for radial legs 29 and 65, smoothed in radius with the Bartlett filter described in section 3. In each case, the RMSC is located within 3 km of both the radius of maximum upward motion and the radius of maximum relative vorticity. Examining all 86 individual radial legs, it was found that the RMSC was within 3 km of the radius of the absolute maximum updraft 42% of time, and located within 3 km of a local updraft maximum in 82% of the radial legs. Similarly, in 85% of radial legs the RMSC was within 3 km of a local relative vorticity maximum, and was located within 3 km of the absolute relative vorticity maximum 53% of the time.

It was shown in section 4 that the RMSC is nearly

equivalent to the radii of maximum upward motion and relative vorticity in each of the five composite time periods, providing dynamical significance to the RMSC. The radius of maximum updraft or relative vorticity were themselves not chosen to composite on because these fields are two of the noisiest and highly variable flight-level quantities, with the largest updraft velocities and biggest values of vorticity (produced by small-scale bumps in the tangential wind profile) sometimes associated with the inner rainbands, far removed from the eyewall.

Figure B2 shows the temporal variability of the (a) RMW and (b) RMSC by radial leg and plotted based upon the geographical quadrant the leg traversed. As was discussed above, the RMW and RMSC are often noted to be 25+ km apart due to the flat wind profiles and secondary wind maxima seen on 31 August (legs

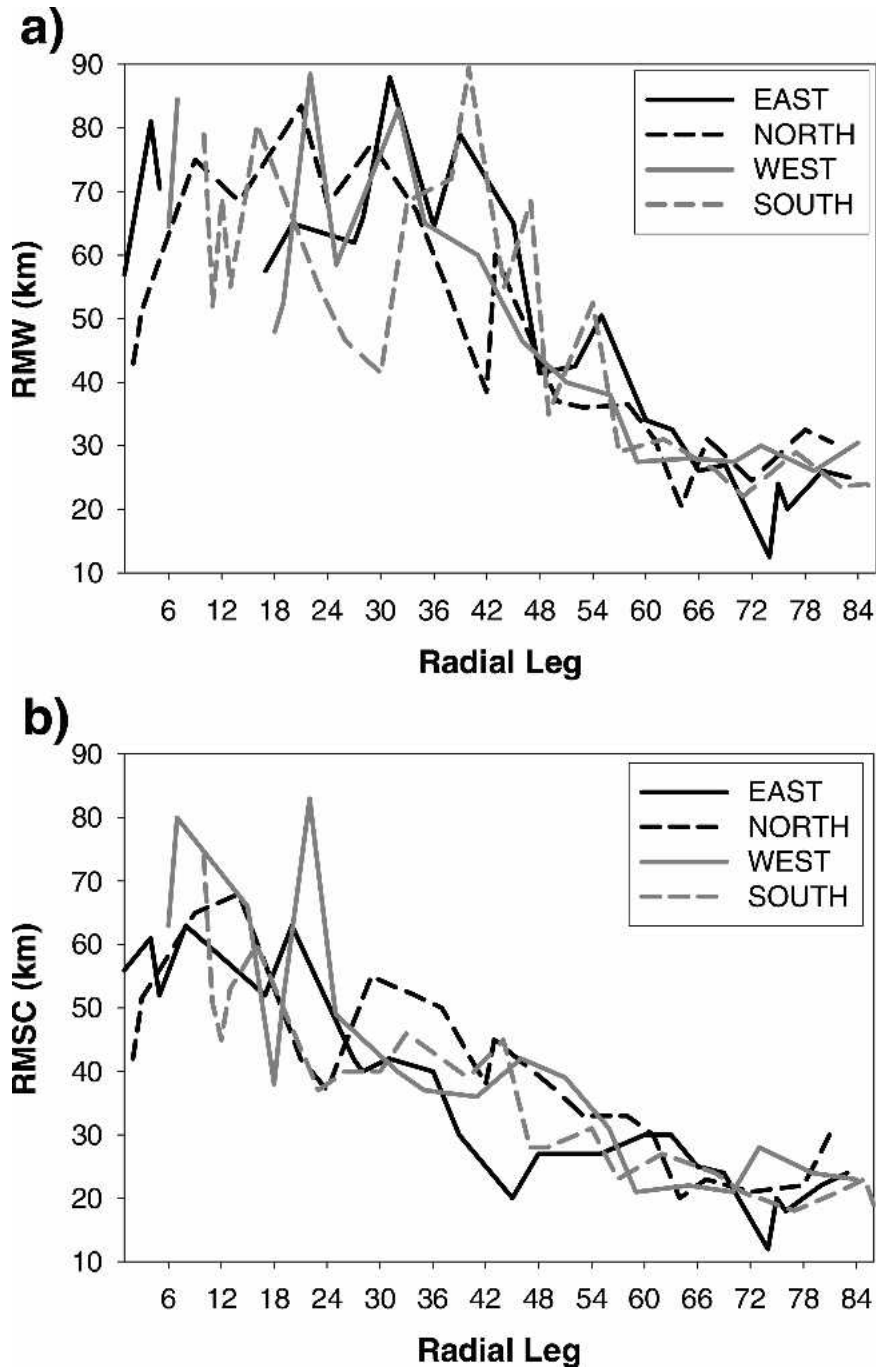


FIG. B2. Line graphs illustrating the temporal changes in (a) the radius of maximum tangential wind and (b) the radius of maximum slope change, grouped according to which quadrant each radial leg passed through.

1–42). Figure B2a shows that the RMW can vary as much as 40 km between legs only 2 h apart into the same storm quadrant. With the exception of legs that investigated the western quadrant of Elena, the variability of the RMSC (Fig. B2b) is much smaller compared to that of the RMW.

REFERENCES

Black, M. L., R. W. Burpee, and F. D. Marks Jr., 1996: Vertical motion characteristics of tropical cyclones determined with airborne Doppler radial velocities. *J. Atmos. Sci.*, **53**, 1887–1909.

Black, R. A., H. B. Bluestein, and M. L. Black, 1994: Unusually

- strong vertical motions in a Caribbean hurricane. *Mon. Wea. Rev.*, **122**, 2722–2739.
- Bolton, D., 1980: The computation of equivalent potential temperature. *Mon. Wea. Rev.*, **108**, 1046–1053.
- Braun, S. A., 2002: A cloud-resolving simulation of Hurricane Bob (1991): Storm structure and eyewall buoyancy. *Mon. Wea. Rev.*, **130**, 1573–1592.
- , and W.-K. Tao, 2000: Sensitivity of high-resolution simulations of Hurricane Bob (1991) to planetary boundary layer parameterizations. *Mon. Wea. Rev.*, **128**, 3941–3961.
- Burpee, R. W., and M. L. Black, 1989: Temporal and spatial variations of rainfall near the centers of two tropical cyclones. *Mon. Wea. Rev.*, **117**, 2204–2218.
- Case, R. A., 1986: Atlantic hurricane season of 1985. *Mon. Wea. Rev.*, **114**, 1390–1405.
- Corbosiero, K. L., and J. Molinari, 2002: The effects of vertical wind shear on the distribution of convection in tropical cyclones. *Mon. Wea. Rev.*, **130**, 2110–2123.
- Davis, C., and L. F. Bosart, 2002: Numerical simulations of the genesis of Hurricane Diana (1984). Part II: Sensitivity of track and intensity prediction. *Mon. Wea. Rev.*, **130**, 1100–1124.
- Eastin, M. D., P. G. Black, and W. M. Gray, 2002a: Flight-level thermodynamic instrument wetting errors in hurricanes. Part I: Observations. *Mon. Wea. Rev.*, **130**, 825–841.
- , —, and —, 2002b: Flight-level thermodynamic instrument wetting errors in hurricanes. Part II: Implications. *Mon. Wea. Rev.*, **130**, 842–851.
- , W. M. Gray, and P. G. Black, 2005: Buoyancy of convective vertical motions in the inner core of intense hurricanes. Part I: General statistics. *Mon. Wea. Rev.*, **133**, 188–208.
- Eliassen, A., 1951: Slow thermally or frictionally controlled meridional circulation in a circular vortex. *Astrophys. Norv.*, **5**, 19–60.
- , and M. Lystad, 1977: The Ekman layer of a circular vortex: A numerical and theoretical study. *Geophys. Norv.*, **31**, 1–16.
- Emanuel, K. A., 1986: An air–sea interaction theory for tropical cyclones. Part I: Steady-state maintenance. *J. Atmos. Sci.*, **43**, 585–604.
- , 1997: Some aspects of hurricane inner-core dynamics and energetics. *J. Atmos. Sci.*, **54**, 1014–1026.
- Frank, W. F., 1984: A composite analysis of the core of a mature hurricane. *Mon. Wea. Rev.*, **112**, 2401–2420.
- Franklin, J. L., S. J. Lord, S. E. Feuer, and F. D. Marks Jr., 1993: The kinematic structure of Hurricane Gloria (1985) determined from nested analyses of dropwindsonde and Doppler radar data. *Mon. Wea. Rev.*, **121**, 2433–2451.
- Hanley, D. E., J., Molinari, and D. Keyser, 2001: A composite study of the interactions between tropical cyclones and upper-tropospheric troughs. *Mon. Wea. Rev.*, **129**, 2570–2584.
- Hawkins, H. F., and D. T. Rubsam, 1968a: Hurricane Hilda, 1964: I. Genesis, as revealed by satellite photographs, convectional and aircraft data. *Mon. Wea. Rev.*, **96**, 428–452.
- , and —, 1968b: Hurricane Hilda, 1964: II. Structure and budgets of the hurricane on October 1, 1964. *Mon. Wea. Rev.*, **96**, 617–636.
- , and —, 1968c: Hurricane Hilda, 1964: III. Degradation of the hurricane. *Mon. Wea. Rev.*, **96**, 701–707.
- , and S. M. Imbembo, 1976: The structure of a small, intense Hurricane-Inez 1966. *Mon. Wea. Rev.*, **104**, 418–442.
- Houze, R. A., Jr., 1993: *Cloud Dynamics*. Academic Press, 573 pp.
- Jenkins, G. M., and D. G. Watts, 1968: *Spectral Analysis and Its Applications*. Holden-Day, 525 pp.
- Jorgensen, D. P., 1984a: Mesoscale and convective scale characteristics of mature hurricanes. Part I: General observations by research aircraft. *J. Atmos. Sci.*, **41**, 1267–1285.
- , 1984b: Mesoscale and convective scale characteristics of mature hurricanes. Part II: Inner core structure of Hurricane Allen (1980). *J. Atmos. Sci.*, **41**, 1287–1311.
- , E. J. Zipser, and M. A. LeMone, 1985: Vertical motion characteristics in intense hurricanes. *J. Atmos. Sci.*, **42**, 839–856.
- Kossin, J. P., and M. D. Eastin, 2001: Two distinct regimes in the kinematic and thermodynamic structure of the hurricane eye and eyewall. *J. Atmos. Sci.*, **58**, 1079–1090.
- Liu, Y., D.-L. Zhang, and M. K. Yau, 1999: A multiscale numerical study of Hurricane Andrew (1992). Part II: Kinematics and inner-core structures. *Mon. Wea. Rev.*, **127**, 2597–2616.
- Marks, F. D., Jr., 1985: Evolution of the structure of precipitation in Hurricane Allen (1980). *Mon. Wea. Rev.*, **113**, 909–930.
- , and R. A. Houze Jr., 1987: Inner core structure of Hurricane Alicia from airborne Doppler radar observations. *J. Atmos. Sci.*, **44**, 1296–1317.
- , —, and J. F. Gamache, 1992: Dual-aircraft investigation of the inner core of Hurricane Norbert. Part I: Kinematic structure. *J. Atmos. Sci.*, **49**, 919–942.
- Molinari, J., and D. Vollaro, 1989: External influences on hurricane intensity. Part I: Outflow layer eddy momentum fluxes. *J. Atmos. Sci.*, **46**, 1093–1105.
- , and —, 1990: External influences on hurricane intensity. Part II: Vertical structure and response of the hurricane vortex. *J. Atmos. Sci.*, **47**, 1902–1918.
- , S. Skubis, and D. Vollaro, 1995: External influences on hurricane intensity. Part III: Potential vorticity structure. *J. Atmos. Sci.*, **52**, 3593–3606.
- Montgomery, M. T., H. D. Snell, and Z. Yang, 2001: Axisymmetric spin-down dynamics of hurricane-like vortices. *J. Atmos. Sci.*, **58**, 421–435.
- Ooyama, K. V., 1969: Numerical simulation of the life-cycle of tropical cyclones. *J. Atmos. Sci.*, **26**, 3–40.
- Parrish, J. R., R. W. Burpee, F. D. Marks Jr., and R. Grebe, 1982: Rainfall patterns observed by digitized radar during the land-fall of Hurricane Frederic (1979). *Mon. Wea. Rev.*, **110**, 1933–1944.
- Pu, Z., W.-K. Tao, S. Braun, J. Simpson, Y. Jia, J. Halverson, W. Olson, and A. Hou, 2002: The impact of TRMM data on mesoscale numerical simulation of Supertyphoon Paka. *Mon. Wea. Rev.*, **130**, 2448–2458.
- Reasor, P. D., M. T. Montgomery, F. D. Marks Jr., and J. F. Gamache, 2000: Low-wave number structure and evolution of the hurricane inner core observed by airborne dual-Doppler radar. *Mon. Wea. Rev.*, **128**, 1653–1680.
- Riehl, H., 1950: A model for hurricane formation. *J. Appl. Phys.*, **21**, 917–925.
- Rogers, R., S. Chen, J. Tenerelli, and H. Willoughby, 2003: A numerical study of the impact of vertical wind shear on the distribution of rainfall in Hurricane Bonnie (1998). *Mon. Wea. Rev.*, **131**, 1577–1599.
- Schubert, W. H., M. T. Montgomery, R. K. Taft, T. A. Guinn, S. R. Fulton, J. P. Kossin, and J. P. Edwards, 1999: Polygonal eyewalls, asymmetric eye contraction, and potential vorticity mixing in hurricanes. *J. Atmos. Sci.*, **56**, 1197–1223.
- Shapiro, L. J., and H. E. Willoughby, 1982: The response of balanced hurricanes to local sources of heat and momentum. *J. Atmos. Sci.*, **39**, 378–394.
- Shea, D. J., and W. M. Gray, 1973: The hurricane's inner core region. I. Symmetric and asymmetric structure. *J. Atmos. Sci.*, **30**, 1544–1564.
- Velden, C. S., 1987: Satellite observations of Hurricane Elena

- (1985) using the VAS $6.7 \mu\text{m}$ "water vapor" channel. *Bull. Amer. Meteor. Soc.*, **68**, 210–215.
- Willoughby, H. E., 1990: Temporal changes of the primary circulation in tropical cyclones. *J. Atmos. Sci.*, **47**, 242–264.
- , 1998: Tropical cyclone eye thermodynamics. *Mon. Wea. Rev.*, **126**, 3053–3067.
- , and M. B. Chelmow, 1982: Objective determination of hurricane tracks from aircraft observations. *Mon. Wea. Rev.*, **110**, 1298–1305.
- , J. A. Clos, and M. G. Shoreibah, 1982: Concentric eyewalls, secondary wind maxima, and the evolution of the hurricane vortex. *J. Atmos. Sci.*, **39**, 395–411.
- , F. D. Marks Jr., and R. J. Feinberg, 1984: Stationary and moving convective bands in hurricanes. *J. Atmos. Sci.*, **41**, 3189–3211.
- Wu, L., S. Braun, J. Halverson, and G. Heymsfield, 2005: A numerical study of Hurricane Erin (2001). Part I: Model verification and storm evolution. *J. Atmos. Sci.*, in press.
- Yau, M. K., Y. Liu, D.-L. Zhang, and Y. Chen, 2004: A multiscale numerical study of Hurricane Andrew (1992). Part VI: Small-scale inner-core structures and wind streaks. *Mon. Wea. Rev.*, **132**, 1410–1433.
- Zipser, E. J., R. J. Meitin, and M. A. LeMone, 1981: Mesoscale motion fields associated with a slowly moving GATE convective band. *J. Atmos. Sci.*, **38**, 1725–1750.